Journal for Geometry and Graphics
Volume 20 (2016), No. 2, 225–241.

# Two Examples of Solids Constructed From Given Developments

**Hellmuth Stachel**

*Institute of Discrete Mathematics and Geometry, Vienna University of Technology*
*Wiedner Hauptstr. 8-10/104, A-1040 Vienna, Austria*
*email:* stachel@dmg.tuwien.ac.at

**Abstract.** The paper provides two examples, where the bending of a planar area $\Phi_0$ with boundary $c_0$ generates a developable surface patch $\Phi$ bounded by a particular spatial curve $c$. There are various ways to restrict such bendings. In the first example the surface $\Phi$ is a cylinder with given rulings, and the spatial counterpart $c$ of the boundary $c_0$ is planar. In the second example the rulings are unknown. Instead of this constraint, the closed boundary $c_0$ is subdivided into two subarcs which are glued together while $\Phi_0$ is bent. In both examples we obtain solids enclosed by torses with geodesic circles $c$ as curved edges.

*Key Words:* surfaces of constant curvature, curved folding, developable surfaces, geodesic circle

*MSC 2010:* 53A03, 51M04, 51N05, 68U07

## 1. First example, a cylindrical box

A very common way of producing small boxes in shops or in fast-food restaurants is to push up special planar cardbord forms with prepared creases. For the case of creases along circular arcs $c_0$ (see Figure 1, left), W. Wunderlich pointed out in [13] that at the spatial form the creases are again planar (see Figure 1, right). They belong to a family $\mathcal{F}$ of curves which are well-known in differential geometry since C. F. Gauss: the curves are meridians of surfaces of revolution with constant Gaussian curvature. The family $\mathcal{F}$ includes circular arcs, since spheres have a constant curvature, too. This stimulates to reflect about a generalization of Wunderlich's result (compare with Theorem 1).

### 1.1. Surfaces of revolution with constant Gaussian curvature

To begin with, we recall the classification of the curves of $\mathcal{F}$: Let the meridian $c$ in the $xy$-plane with the twice-differentiable arc-length parametrization

$$\mathbf{c}(s) = (x(s),\, y(s)) \ \text{ for } s_1 \le s \le s_2$$

ISSN 1433-8157/\$ 2.50 

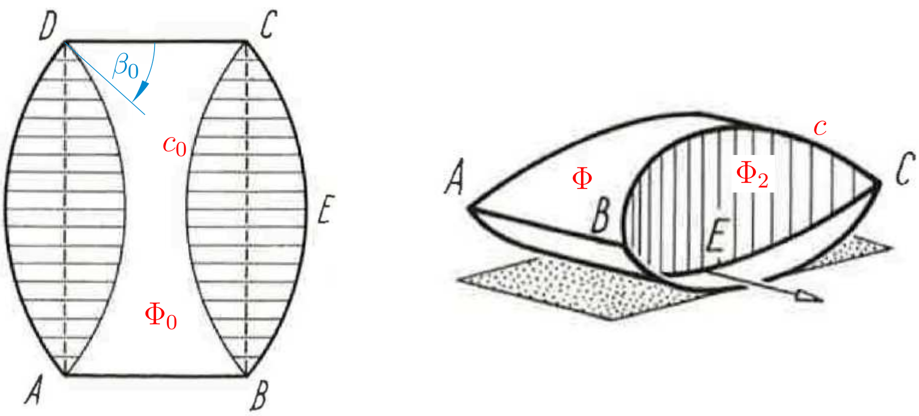


Figure 1: WUNDERLICH's original figure in [13]: development (left) and spatial form (right), both with supplementary labels

rotate about the $x$-axis (Figure 2). If primes indicate the differentiation with respect to (w.r.t. in short) the arc-length $s$ then $\mathbf{c}' = (x',\, y') = (\cos\alpha,\, \sin\alpha)$ is the unit tangent vector and $\mathbf{c}'' = (x'',\, y'') = \kappa_1(y', -x')$ the curvature vector.

At surfaces of revolution, the meridians and parallel circles are the principal curvature lines. Therefore, the signed principal curvatures at the point $P = \mathbf{c}(s)$ are

$$\kappa_1 = -\frac{y''}{\cos\alpha}, \quad \kappa_2 = \frac{\cos\alpha}{y}$$

(see Figure 2, where $\rho_i = 1/\kappa_i$). The Gaussian curvature $K = \kappa_1\kappa_2$ is constant if and only if the meridian $c$ satisfies the differential equations

$$y'' + Ky = 0, \quad x' = \sqrt{1 - y'^2} \tag{1}$$

with $K = \text{const.}$, provided that $\cos\alpha \neq 0$.

In the case $K = 0$ the meridians are lines; the corresponding surfaces of revolution are

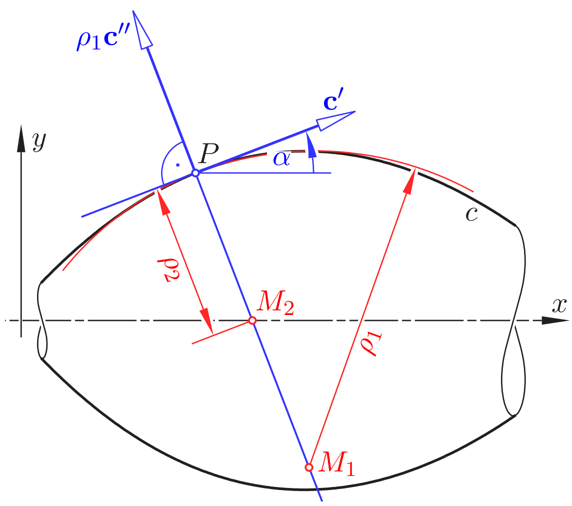


Figure 2: $M_1$ and $M_2$ are the Meusnier centers of the principal curvature lines at point $P \in c$

Table 1: Meridians of the surfaces of revolution with constant Gaussian curvature $K$ (see Figure 3).

| | *curvature* | *coefficients in* (2) | *name* |
|---|---|---|---|
| 1. | $K = 1$ | $0 < a < 1,\ b = 0$ | spindle type (elliptic) |
| 2. | | $a = 1,\ b = 0$ | sphere (parabolic) |
| 3. | | $a > 1,\ b = 0$ | bulge type (hyperbolic) |
| 4. | $K = -1$ | $a = 0,\ 0 < b < 1$ | cone type (elliptic) |
| 5. | | $b = a = 1$ | tractrix (parabolic) |
| 6. | | $a > 0,\ b = 0$ | gorge type (hyperbolic) |

right cones or cylinders. In the remaining cases $K \neq 0$ we obtain the general solutions

$$\begin{aligned} K > 0: &\quad y = a\cos s\sqrt{K} + b\sin s\sqrt{K}, \\ K < 0: &\quad y = a\cosh s\sqrt{-K} + b\sinh s\sqrt{-K}, \end{aligned} \tag{2}$$

with constant $a, b \in \mathbb{R}$, and $x = \int \sqrt{1 - y'^2}\, ds$.

After specifying an appropriate initial point $s = 0$ for the arc-length parametrization, we can restrict ourselves – up to similarities – to six cases, as listed in Table 1 (see Figure 3 or [7]). This classification dates back to C. F. Gauss (1827) and F. A. Minding (1839) (note [6, p. 277–286], [12, p. 141–148], [9, p. 158] or [2, p. 169]).

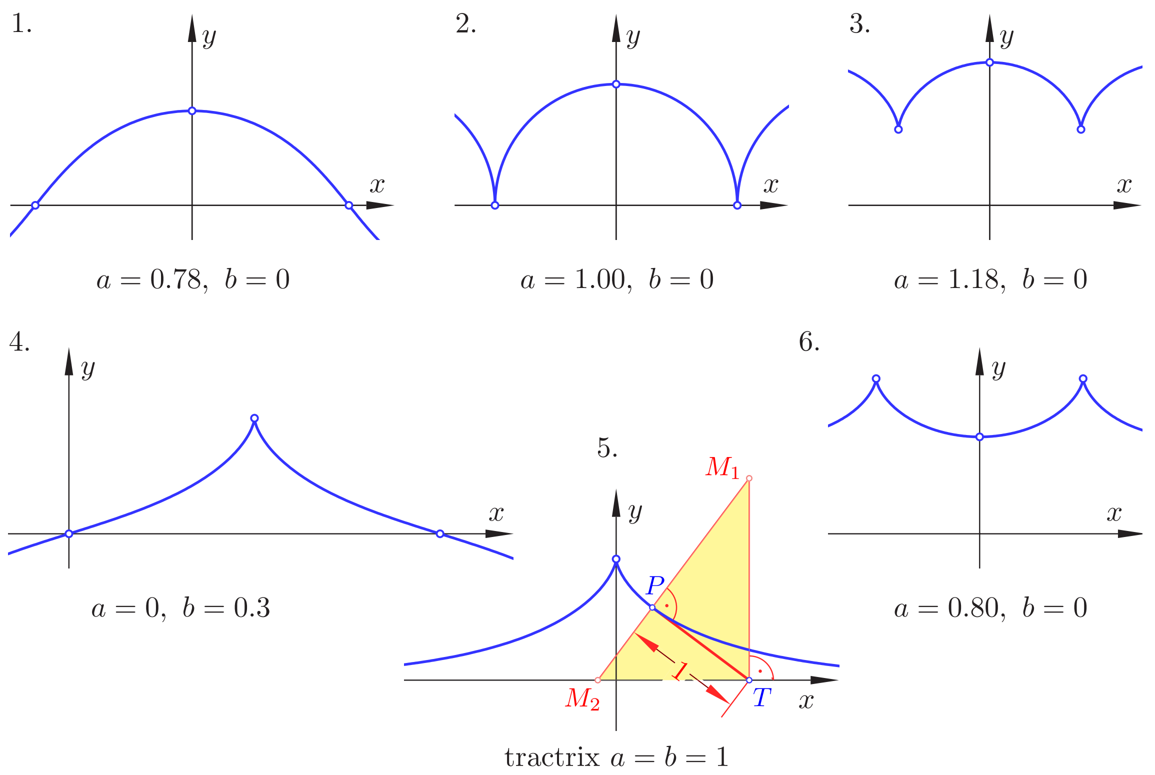


Figure 3: Curves of the family $\mathcal{F}_0$ of meridians of surfaces of revolution with constant Gaussian curvature $K = 1$ (top row) and $K = -1$ (bottom row)

In case 2 the meridian $c$ is a half-circle centered on the $x$-axis. Due to G. Scheffers [11], the curve $c$ of case 1 shows up at the development of an elliptic cylinder when bounded by a circular section. This can easily be verified by comparison with the first equation in (2). The meridian $c$ in case 5 has the arc-length parametrization

$$x = \sqrt{1 - e^{-2s}} - \operatorname{arcosh} e^s, \;\; y = e^{-s}, \quad s > 0\,.$$

This defines a *tractrix*, since the segment between $P \in c$ and the meet $T$ of the tangent at $P$ and the $x$-axis has the constant length 1. The corresponding surface of revolution is called *pseudosphere* (or bugle surface or tractroid).

*Remark* 1. According to [4], the curves of the family $\mathcal{F}$ in the cases 1 and 3 serve as center curves of a rolling unit disk which moves such that an excentric point attached to the disk traces a straight line. We can verify this in the following way: Let the moving plane rotate with angular velocity 1 around any point $M$, which simultaneously moves with unit-speed along a curve $(x(s),\, y(s))$. Then the moving polode must be the unit circle, and the trajectory of the point with coordinates $(x_1, y_1)$ w.r.t. the moving plane is given by

$$\begin{pmatrix} x_0 \\ y_0 \end{pmatrix} = \begin{pmatrix} x(s) \\ y(s) \end{pmatrix} + \begin{pmatrix} \cos s & \sin s \\ -\sin s & \cos s \end{pmatrix} \begin{pmatrix} x_1 \\ y_1 \end{pmatrix}.$$

If, according to (2), we specify $y(s) = a\cos s$ and set $(x_1, y_1) = (0, -a)$ we obtain directly $y_0 = 0$. By the same token, a similar property of the curves in the cases 4–6 can be verified in the complex extension by specifying the angular velocity as $i$ (= imaginary unit).

### 1.2. Curved edge at the bending of a planar ruled surface

**Theorem 1.** *Let $\mathcal{F}_0$ be the family of meridians of surfaces of revolution with constant Gaussian curvature $K \neq 0$. Suppose a curve $c_0 \in \mathcal{F}_0$ bounds together with the corresponding axis $a_0$ (= $x$-axis) the development $\Phi_0$ of a cylindrical patch with generators orthogonal to $a_0$.*
*If at a cylindrically bent pose $\Phi$ of $\Phi_0$ the corresponding boundary curve $c$ is located in a plane $\varepsilon$ then $c$ is again a member of the family $\mathcal{F}_0$ and even with the same curvature $K$. The axis of $c$ is the meet of $\varepsilon$ and the plane of the orthogonal section $a$, which is the bent counterpart of the original axis $a_0$.*

*Proof.* There is an isometry between the flat initial pose $\Phi_0$ and the cylindrical shape $\Phi$. Therefore the arc-length $s$ of $c_0$ serves also as arc-length of $c \subset \varepsilon$. If at the bent pose $\Phi$ the line of intersection between $\varepsilon$ and the plane of the cross section $a$ is used as $x$-axis then the original $y_0$-coordinate of any point $P_0 \in c_0$ and the $y$-coordinate of the corresponding point $P \in c$ satisfy

$$y_0(s) = y(s)\cos\beta, \tag{3}$$

where the constant $\beta$ with $0 < \beta \leq \frac{\pi}{2}$ denotes the angle of inclination of the generators of $\Phi$ w.r.t. the plane $\varepsilon$ (Figure 4). We have $\beta < \frac{\pi}{2}$ since otherwise $c_0$ would be a line.
The $y$-coordinate $y_0(s)$ of the given boundary curve $c_0$ satisfies (1). Consequently, the planar section $c$ of $\Phi$ satisfies the same equation $y'' + Ky = 0$. This means in particular that the Gaussian curvature $K$ of the corresponding surfaces of revolution is preserved.
If we plug (3) into the general solutions $y_0 = y_0(s)$, as listed in (2), the coefficients $a_0, b_0$ are replaced with

$$a = \frac{a_0}{\cos\beta} \geq a_0 \quad \text{and} \quad b = \frac{b_0}{\cos\beta} \geq b_0. \tag{4}$$

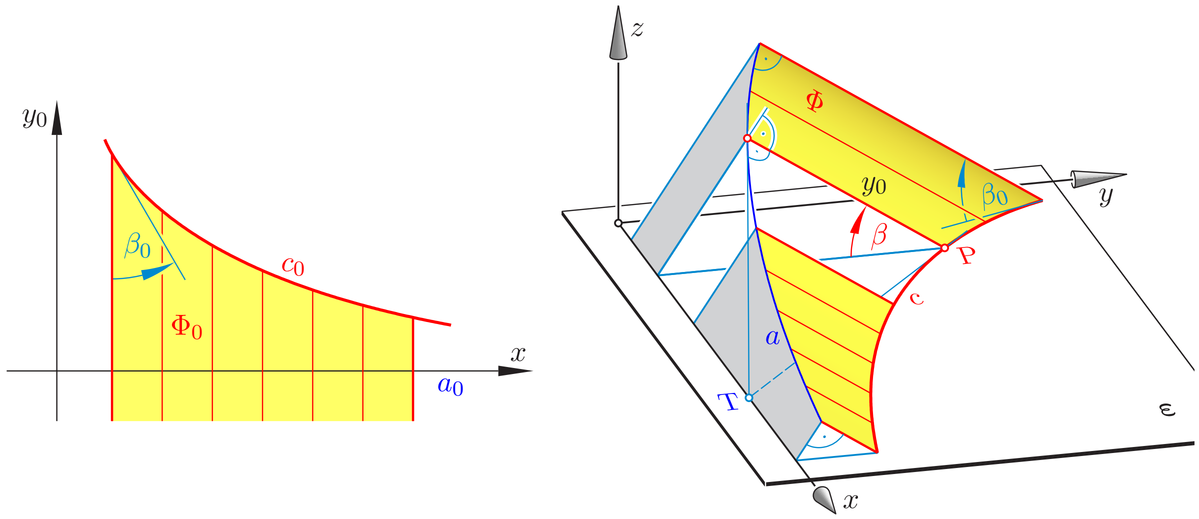


Figure 4: $\Phi_0$ with boundary $c_0 \in \mathcal{F}_0$ is cylindrically bent with a planar boundary $c$

Hence, if $c_0$ is of type 2 like in Figure 1 then $c$ is of type 3. The question why the boundary curve $c$ must be planar will be addressed below in Theorem 3.

For $c_0$ of type 3 the curve $c$ is again of type 3, while the bending of $c_0$ of type 1 results in curves $c$ of types 1, 2[1] or 3. Finally, each of the types 4, 5 and 6 is preserved. □

We can perform a continuous bending from $\Phi_0$ to $\Phi$ by varying the inclination angle $\beta$. The condition $|dy/ds| = |y'| \leq 1$, by virtue of (1), implies an upper limit $\beta_0$ for $\beta$, i.e.,

$$0 \leq \beta \leq \beta_0.$$

Also Figure 4 reveals that the angle $\beta$ of inclination cannot be bigger than the angles between the generators and the boundary $c_0$ in the initial flat pose.

**Corollary 2.** *A bent pose $\Phi$, as described in Theorem 1, exists only if the angle $\beta$ between the generators of $\Phi$ and the plane $\varepsilon$ is smaller of equal to the smallest angle $\beta_0$ between the generators and the boundary curve $c_0$ in the development $\Phi_0$.*
*If $c_0$ lies on a tractrix then $c$ is congruent to another portion of the same tractrix.*

*Proof.* The second statement is a consequence of (4) under the condition $a_0 = b_0$, since $a = b$ characterizes tractrices among the curves of the family $\mathcal{F}_0$, i.e., case 5 in Table 1. However, this statement follows also from the invariance of the distance $\overline{PT}$ along the tangent from the point $P \in c_0$ to the intersection $T$ with the $x$-axis (see Figures 3 and 4). □

Concerning the planarity of the crease $c$ in Figure 1, we focus on a generalization, which is already mentioned in [13, p. 114], however without a proof. Let

$$\mathbf{x}_0 \colon \begin{cases} I \times \mathbb{R} \to \mathbb{R}^2, \\ (s,t) \ \mapsto \mathbf{x}_0(s,t) = \mathbf{c}_0(s) + t\,\mathbf{r}_0(s) \end{cases} \tag{5}$$

be a $C^2$-parametrization of a planar ruled surface (Figure 5). We specify $\mathbf{c}_0(s)$ as arc-length parametrization of a plane curve $c_0$ and $\mathbf{r}_0(s)$ as normalized direction vector of the generator,

[1]This confirms again Scheffers' result in [11] with a circle $c$ and an elliptic cylinder $\Phi$.

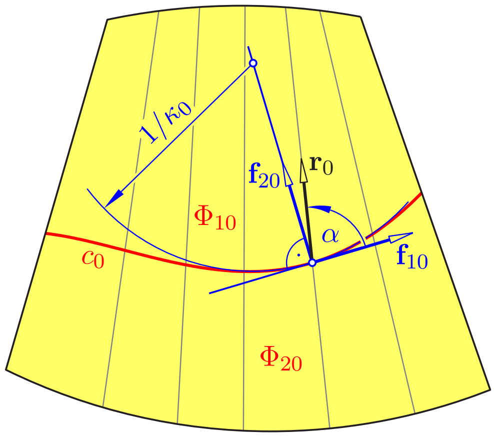


Figure 5: Theorem 3 deals with a bent pose of this development such that $c_0$ becomes a proper edge between the torses with given developments $\Phi_{10}$ and $\Phi_{20}$

i.e., $\|\mathbf{r}_0(s)\| = \|\mathbf{c}_0'\| = 1$ for all $s \in I$. Furthermore we assume that $c_0$ is nowhere tangent to any generator.

Let $\Phi_0$ be a sufficiently small subarea of this planar 'ruled surface' such that the parametrization (5) is injective and $c_0$ subdivides $\Phi_0$ into two patches $\Phi_{10}$ and $\Phi_{20}$ (Figure 5). We are interested in bent poses of $\Phi_0$ where the spatial counterpart $c$ of $c_0$ is a proper curved edge between two torses $\Phi_1$ and $\Phi_2$ with generators corresponding to the rulings in the respective developments $\Phi_{10}$ and $\Phi_{20}$. Then we can state:

**Theorem 3.** *If the two adjacent patches $\Phi_{10}$ and $\Phi_{20}$ of the planar ruled surface, as defined above, are the developments of two developable patches $\Phi_1$ and $\Phi_2$ with a proper curved edge $c$ between them, this crease $c$ must be a planar curve. The two torses, which arise by extending all generators of the patches $\Phi_1$ and $\Phi_2$ to full lines, are symmetric w.r.t. the plane of $c$.*[2]

*Proof.* Let $(\mathbf{f}_1, \mathbf{f}_2, \mathbf{f}_3)$ be the Frenet frame of the crease $c$ with the arc-length parametrization $\mathbf{c}(s)$ and the Frenet equations

$$\begin{aligned} \mathbf{f}_1' &= \phantom{-\kappa\,\mathbf{f}_1} \kappa\,\mathbf{f}_2\,, \\ \mathbf{f}_2' &= -\kappa\,\mathbf{f}_1 \phantom{\kappa\,\mathbf{f}_2} + \tau\,\mathbf{f}_3\,, \\ \mathbf{f}_3' &= \phantom{-\kappa\,\mathbf{f}_1} -\tau\,\mathbf{f}_2\,. \end{aligned}$$

The continuous process of bending induces, at each instant, an orientation preserving isometry

$$\mathbf{x}_0(s,t) \;\mapsto\; \mathbf{c}(s) + t\,\mathbf{r}_i$$

between the patch $\Phi_{i0}$ of the planar ruled surface in (5) and the curved patch $\Phi_i$, for each $i \in \{1,2\}$. Therefore, the signed curvature $\kappa_0$ of $c_0$ equals the geodesic curvature $\kappa_{gi}$ of $c$ w.r.t. $\Phi_i$. In addition, for all $s \in I$ the angle $\alpha(s)$ between $\mathbf{c}_0'(s) = \mathbf{f}_{10}$ and the generator $\mathbf{r}_0(s)$ remains unchanged (see Figure 5).

On the other hand, the curve $c$ defines a right-handed Darboux frame $(\mathbf{d}_{1i}, \mathbf{d}_{2i}, \mathbf{d}_{3i})$ on each torse $\Phi_i$, $i = 1,2$, consisting of the tangent unit vector $\mathbf{d}_{1i} = \mathbf{f}_1 = \mathbf{c}'$, the normal unit vector $\mathbf{d}_{2i}$ within the tangent plane of $\Phi_i$ and the normalized surface normal $\mathbf{d}_{3i} = \mathbf{d}_{1i} \times \mathbf{d}_{2i}$. During

[2] In Origami, the transition from the extension of $\Phi_1$ to $\Phi_2$ is called *reflection operation* (see, e.g., [10, p. 187]).

the continuous bending from $\Phi_{i0}$ to $\Phi_i$, the isometries transform the 2-dimensional Frenet frame $(\mathbf{f}_{10}, \mathbf{f}_{20})$ of $c_0$ into the pair $(\mathbf{d}_{1i}, \mathbf{d}_{2i})$ for all $s \in I$. Hence, the orientation of the surface normal $\mathbf{d}_{3i}$ of $\Phi_i$ is uniquely defined.

The derivatives of the vectors of the Darboux frames satisfy, for $i = 1, 2$,

$$\begin{array}{rcrrr} \mathbf{d}'_{1i} & = & & \kappa_{gi}\,\mathbf{d}_{2i} & +\kappa_{ni}\,\mathbf{d}_{3i}\,, \\ \mathbf{d}'_{2i} & = & -\kappa_{gi}\,\mathbf{d}_{1i} & & +\tau_{gi}\,\mathbf{d}_{3i}\,, \\ \mathbf{d}'_{3i} & = & -\kappa_{ni}\,\mathbf{d}_{1i} & -\tau_{gi}\,\mathbf{d}_{2i}\,. & \end{array}$$

At each point of $c$ we can transform the Frenet frame of $c$ into the Darboux frame w.r.t. $\Phi_i$ by a rotation about the tangent vector $\mathbf{d}_{1i} = \mathbf{f}_1$. Let $\gamma_i(s)$ denote the angle of this rotation. Then, for each $s \in I$,

$$\mathbf{d}_{1i} = \mathbf{f}_1, \quad \begin{array}{rcl} \mathbf{d}_{2i} & = & \cos\gamma_i\,\mathbf{f}_2 - \sin\gamma_i\,\mathbf{f}_3\,, \\ \mathbf{d}_{3i} & = & \sin\gamma_i\,\mathbf{f}_2 + \cos\gamma_i\,\mathbf{f}_3\,. \end{array}$$

These rotations take the osculating plane of $c$ to the tangent planes of the torses $\Phi_1$ and $\Phi_2$, respectively. Now, the invariants of the Darboux frames can be expressed in terms of the invariants of the Frenet frame and the angle $\gamma_i$ as

$$\kappa_{gi} = \kappa\cos\gamma_i\,, \quad \kappa_{ni} = \kappa\sin\gamma_i\,, \quad \tau_{gi} = \tau - \gamma'_i\,. \tag{6}$$

Because of $\kappa_{g1} = \kappa_{g2} = \kappa_0$ at each point $\mathbf{c}(s)$, the cosines of $\gamma_1$ and $\gamma_2$ equal $\kappa_0/\kappa$. Since there must be a proper edge along the crease $c$ between $\Phi_1$ and $\Phi_2$, the angles $\gamma_1$ and $\gamma_2$, when restricted by $-\pi < \gamma_i \le \pi$, must have different signs, i.e., $\gamma_2 = -\gamma_1 \ne 0$.
Torses are the envelopes of their tangent planes. Therefore, the generator of $\Phi_i$ at $\mathbf{c}(s)$ has the direction of

$$\mathbf{d}_{3i} \times \mathbf{d}'_{3i} = \tau_{gi}\,\mathbf{d}_{1i} - \kappa_{ni}\,\mathbf{d}_{2i} = (\tau - \gamma'_i)\mathbf{d}_{1i} - \kappa\sin\gamma_i\,\mathbf{d}_{2i}\,.$$

The oriented angle $\alpha$ between the tangent vector $\mathbf{d}_{1i}$ and the generator $\mathbf{r}_i$ shows already up in the development (see Figure 5). Since this angle is the same for both developable patches, we obtain

$$\cos\alpha : \sin\alpha = (\tau - \gamma'_1) : (-\kappa\sin\gamma_1) = (\tau - \gamma'_2) : (-\kappa\sin\gamma_2) = (\tau + \gamma'_1) : \kappa\sin\gamma_1\,.$$

The curve $c_0$ was supposed to be transversal to the rulings. Therefore we have $\sin\alpha \ne 0$ everywhere, and consequently

$$(\tau - \gamma'_1) = -(\tau + \gamma'_1), \text{ hence } \tau = 0.$$

The crease $c$ must be planar. When at each point of $c$ the tangent planes of $\Phi_1$ and $\Phi_2$ are symmetric w.r.t. the plane of $c$, then $\Phi_1$ and $\Phi_2$ are patches of two symmetric torses.

At the end of this proof, two comments on excluded cases: If the crease is not a proper edge between $\Phi_1$ and $\Phi_2$ then $\gamma_1 = \pm\frac{\pi}{2}$ or $\gamma_1 = 0$ for all $s \in I$. In the first case the two patches belong to the same torse, $c$ is a geodesic on this torse, and $c_0$ is aligned, i.e., $\kappa_0 = 0$. In the second case the crease $c$ is the cuspidal edge, and $\Phi_1$ and $\Phi_2$ belong to the two sheets of the tangent surface of $c$. In both cases, $c$ needs not be planar. □

At the box displayed in Figure 1 the planar ruled surface given in (5) has parallel generators, i.e., $\mathbf{r}_0(s) = \text{const.}$, and we have $\beta = \frac{\pi}{4}$ in (4) and Figure 4. Due to Corollary 2, in the

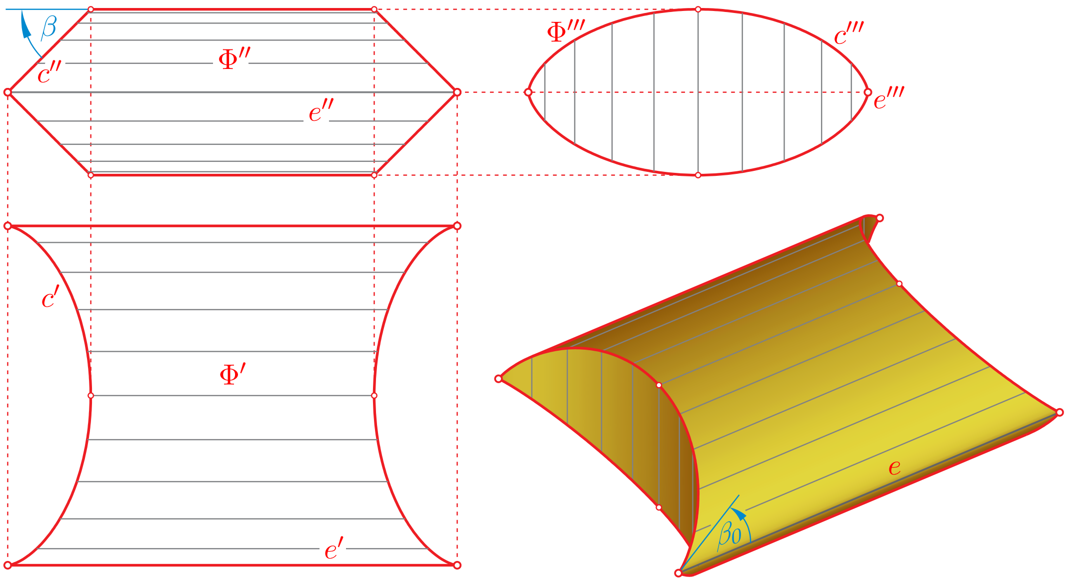


Figure 6: Views of the cylindrical box in the extreme case $\beta_0 = \beta = 45°$

development the minimum angle $\beta_0$ between the generators and curve $c_0$ cannot be smaller than $\pi/4$. Figure 6 shows a box (with the bottom face congruent to the top face $\Phi$) in the limit case $\beta_0 = \frac{\pi}{4}$. Therefore the interior angles at two vertical digons (hatched in Figure 1) reach the possible maximum $\frac{\pi}{2}$. The common generator $e$ between the top face $\Phi$ and the bottom face is no longer an edge like in Figure 1, but both cylinders share a vertical tangent plane along $e$.

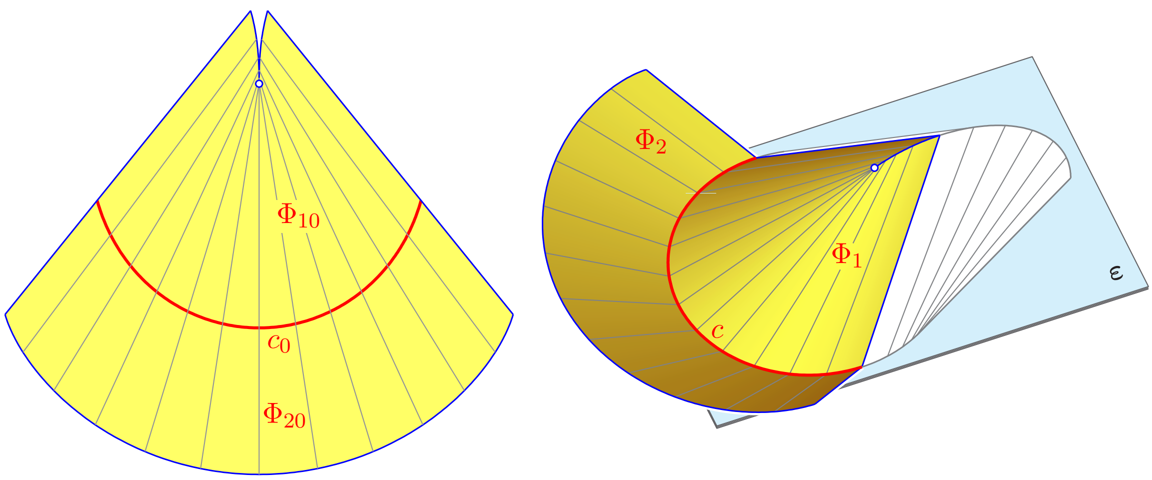


Figure 7: This example to Theorem 3 is related to an Oloid and its extension

Another example of Theorem 3 is shown in Figure 7. This time the developable patch $\Phi_1$ is a general torse, namely a portion of the boundary of the *Oloid*, which is defined as the convex hull of two circles in orthogonal planes such that each circle contains the center of the other circle (see, e.g., [5]). One of these circles, the circle $c$, separates $\Phi_1$ from the patch $\Phi_2$, which belongs to the socalled *extended Oloid* (note [3]). The plane $\varepsilon$ of $c$ subdivides the Oloid into two symmetric halves. The right picture in Figure 7 shows the upper half of the Oloid with the patch $\Phi_1$ as well as with the patch $\Phi_2$ belonging to the extension of the Oloid's lower half. The development of both patches with the separating curve $c_0$ is displayed on the left hand side.[3]

*Remark* 2. The planarity of the crease $c$, as stated in Theorem 3, is only guaranteed when, in the developments, the generators of $\Phi_{10}$ are aligned with that of $\Phi_{20}$. Without any additional constraints, the bent pose is not rigid. Apart from the continuous bendings obtained by variation of the angle $\gamma$ while each generator remains aligned, also other bendings of $\Phi_1$ and $\Phi_2$ with varying the rulings and a non-planar crease $c$ are possible.

## 2. Second example, a box with a zip

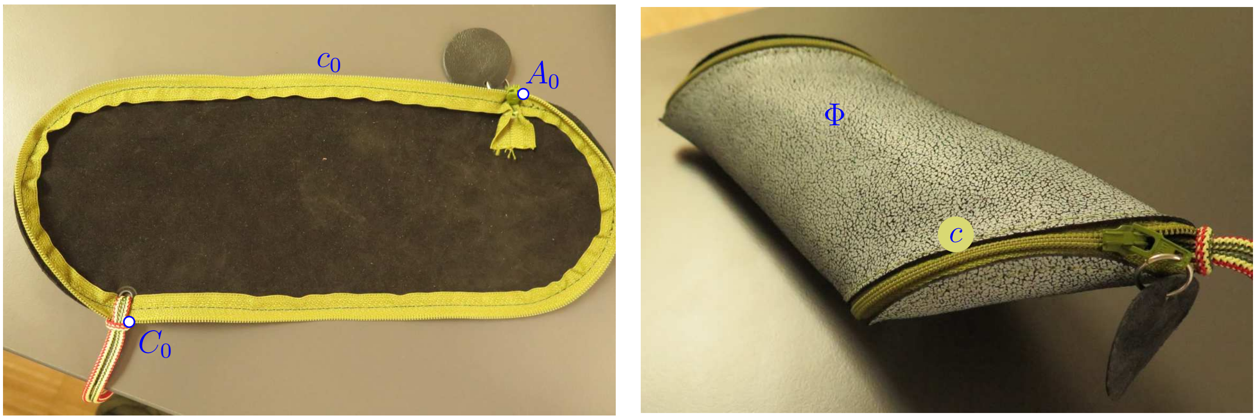


Figure 8: Development and spatial form (photos: G. Glaeser)

At the second example the development $\Phi_0$ is bounded by a $C^1$-curve $c_0$, which is composed from two straight line segments and two semicircles of equal lengths (Figure 8, left). We select two opposite points of transition between semicircles and straight line segments, $A_0$ and $C_0$, for bisecting the boundary. Now the spatial form $\Phi$ is obtained by gluing together, from $A_0$ on, the semicircle of one part with the straight segment of the other, and vice versa (Figure 8, right). The question is, how to model this interesting resulting body?

In contrast to the previous example, the crucial point is here that the rulings are unknown, and local conditions are not sufficient for modelling the bent shape. The constraint is of global nature: the boundary $c_0$ must finally give a two-fold covered closed curve $c$.

In [8] a general and effective algorithm is provided for computing a quad mesh as a discrete model of a developable surface patch which is determined by its development together with a length-preserving mapping between bounding points which have to coincide after bending at the spatial form. Our approach is more geometric but very specific and adjusted to the particular example.

The inspection of a physical model shows:

- The corresponding spatial body with the boundary $\Phi$ is convex and uniquely defined.
- The helix-like curve $c$ is a proper edge of $\Phi$ with the resulting solid as its *convex hull*.
- The spatial body has an axis $a$ of symmetry which connects the spatial counterpart $M$ of the center $M_0$ with the remaining transition point $B = D$ on $c$ (Figure 9).
- The semicircular disks are bent to cones with respective apices $A$ and $C$. Hence, the boundary $\Phi$ is a $C^1$-composition of two cones and a torse between.

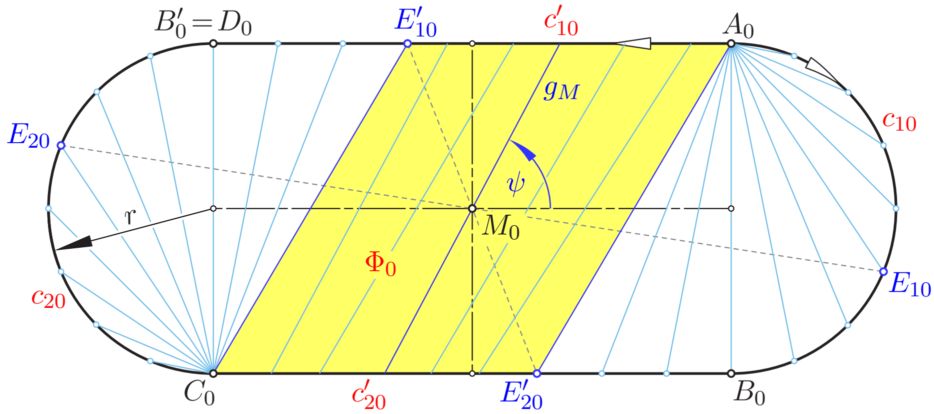


Figure 9: Development for Example 2

We traverse $c$ from $A$ to $C$ and subdivide it at the transition point $B = D$ into the two parts $c_1$ and $c_2$. Then we can state:

**Lemma 4.** *Supposing that the observations of the physical model, as listed above, are correct, the boundary $\Phi$ of the convex solid has the following properties:*

1. *The rotation about the axis $a$ of symmetry through $180°$ maps $\Phi$ onto itself and interchanges $c_1$ and $c_2$. Hence, $a$ is orthogonal to the tangent $t_B$ of $c$ at the transition point $B$. The apices $A$ and $C$ are symmetric w.r.t. $a$. The generator $g_M$ of $\Phi$ through the central point $M$ is cylindric[4] and has a tangent plane orthogonal to $a$.*
2. *Because of the straight segments of $c_0$ at the development, the developable surface on the left hand side of $c_1$ belongs to the rectifying torse of $c_1$. With respect to the right hand side, $c_1$ is a geodesic circle of $\Phi$.*
3. *Since at $A_0$ the semicircle is tangent to the adjacent straight segment, the surface $\Phi$ has cone singularities with the intrinsic curvature $\pi$ at the points $A$ and $C$. Therefore, the initial tangent $t_A$ to $c_1$ is a generator of a right cone with apex $A$ and apex angle $60°$. The osculating plane of $c_1$ at $A$ coincides with the cone's tangent plane along $t_A$, and the rectifying plane at $A$ passes through the cone's axis.*

The boundary $\Phi$ with given development $\Phi_0$ belongs to the connecting torse of $c_1$ and $c_2$. If $g$ is a generator of $\Phi$ whose counterpart in the development meets both straight segments of $c_0$ then $g$ meets $c_1$ and $c_2$ at points with parallel and equally oriented tangent vectors. This is since the tangent plane along $g$ must be constant. Hence, we can state

**Lemma 5.** *Under the assumptions of Lemma 4, the boundary $\Phi$ of the convex solid with the curved edge $c = c_1 \cup c_2$ has the following further properties:*

1. *At the point $E_2 \in c_2$ of transition between the cone with apex $A$ and the adjacent torse (see Figure 9) the tangent to $c_2$ must be parallel to the initial tangent $t_A$ to $c_1$ at $A$. The symmetric point $E_1 \in c_1$ has a tangent parallel to the final tangent $t_C$ of $c_2$.*
2. *The tangent indicatrices of $c_1$ and $c_2$ are symmetric w.r.t. a plane orthogonal to the axis $a$. The tangent indicatrices of the subarcs $AE_1 \subset c_1$ and $E_2C \subset c_2$ must coincide (note Figure 11).*

[3]Note that in this example we have $\kappa = \text{const.}$ in (6).

[4]The symmetry w.r.t. $a$ must fix the cuspidal point of $g_M$. Hence, this point either lies at infinity or it coincides with $M$. The latter can be excluded since the velocity vectors of $c_1$ and $c_2$ at their intersections with $g_M$ have the same direction.

*Proof of item 2.* The reflection in $a$ maps $c_1$ onto $c_2$, but reverses the orientation, i.e., reflects on the unit sphere the tangent indicatrix in the center. Therefore the tangent indicatrix of $c_1$ can be transformed into that of $c_2$ by the reflection in a diameter parallel to $a$ followed by the reflection in the center. The product of these reflections is a reflection in the diameter plane orthogonal to $a$. □

### 2.1. A first approximation

We can approximate the requested developable surface $\Phi$ with its self-intersection $c$ by specifying $c_1$ as one half of a geodesic circle on a *right cone* with apex $A$ and apex angle 60°. In this case $\Phi$ is composed of two patches of right cones and a patch of a proper torse between. Though this reflects more or less the shape of a physical model, we will recognize that this cannot be an exact mathematical model.

To begin with, we focus on one half of a geodesic circle $c_1$ on a right cone, whose axis is vertical and whose generators are inclined under 60°. This geodesic circle $c_1$ with radius $r$ is supposed to pass through the cone's apex $A$. We choose a coordinate frame with the cone's axis as $z$-axis and $t_A$ lying in the $xz$-plane (Figure 10). We parametrize the circle $c_1$ by the angle $\varphi$ (with $2\varphi$ being the center angle in the development) and specify $A$ as the point $\varphi = 0$. Then

$$\mathbf{x}(\varphi) = r\left((\sin^2\varphi - \cos^2\varphi)\sin\varphi,\ 2\sin^2\varphi\cos\varphi,\ (1-\sin\varphi)\sqrt{3}\right), \quad 0 \le \varphi \le \frac{\pi}{2}.$$

$\mathbf{x}(\frac{\pi}{2}) = (r, 0, 0)$ is the lowest point $B$ of $c_1$, while $\mathbf{x}(0) = (0, 0, r\sqrt{3})$ coincides with $A$.

The resulting curve $c_1$ is even part of an algebraic curve: In the $xy$-plane, the top view $c_1'$ of $c_1$ is a quarter of a rose curve traced by a point attached to a circle with radius $\frac{r}{6}$, which is rolling outside on a circle of double size:

$$\begin{pmatrix} x \\ y \end{pmatrix} = \frac{r}{2}\begin{pmatrix} \sin\varphi \\ \cos\varphi \end{pmatrix} - \frac{r}{2}\begin{pmatrix} \sin 3\varphi \\ \cos 3\varphi \end{pmatrix}.$$

(The dotted curve in Figure 10 shows the continuation of $c_1'$.) The orthogonal projection of $c_1$ in the $xz$-plane, i.e., the side view $c_1'''$, belongs to a cubic parabola satisfying

$$3x\sqrt{3} = 3(z - \sqrt{3}) - 2(z - \sqrt{3})^3.$$

This cubic parabola has its inflection point at $A_1'''$.

We differentiate $c_1$ w.r.t. its arc-length $s = 2r\varphi$ and get the tangent unit vector

$$\mathbf{t} = \frac{1}{2}\left(5\cos\varphi - 6\cos^3\varphi,\ 4\sin\varphi - 6\sin^3\varphi,\ -\sqrt{3}\cos\varphi\right).$$

The second derivative $\mathbf{x}'' = \mathbf{t}' = \kappa\,\mathbf{n}$ defines the principal normal vector $\mathbf{n}$ and the curvature $\kappa$ of $g$ as

$$\begin{aligned} \kappa &= \frac{1}{2r}\sqrt{4 + 3\sin^2\varphi} \quad \text{and} \\ \mathbf{n} &= \frac{1}{4r\kappa}\left((18\cos^2\varphi - 5)\sin\varphi,\ (4 - 18\sin^2\varphi)\cos\varphi,\ \sqrt{3}\sin\varphi\right). \end{aligned}$$

The second part $c_2$ of the curved edge $c$ is the image of $c_1$ under the half-rotation about an axis $a$ which passes through $B$ and lies in the $xz$-plane. However, the axis $a$ should satisfy simultanously two mutually contradicting conditions:

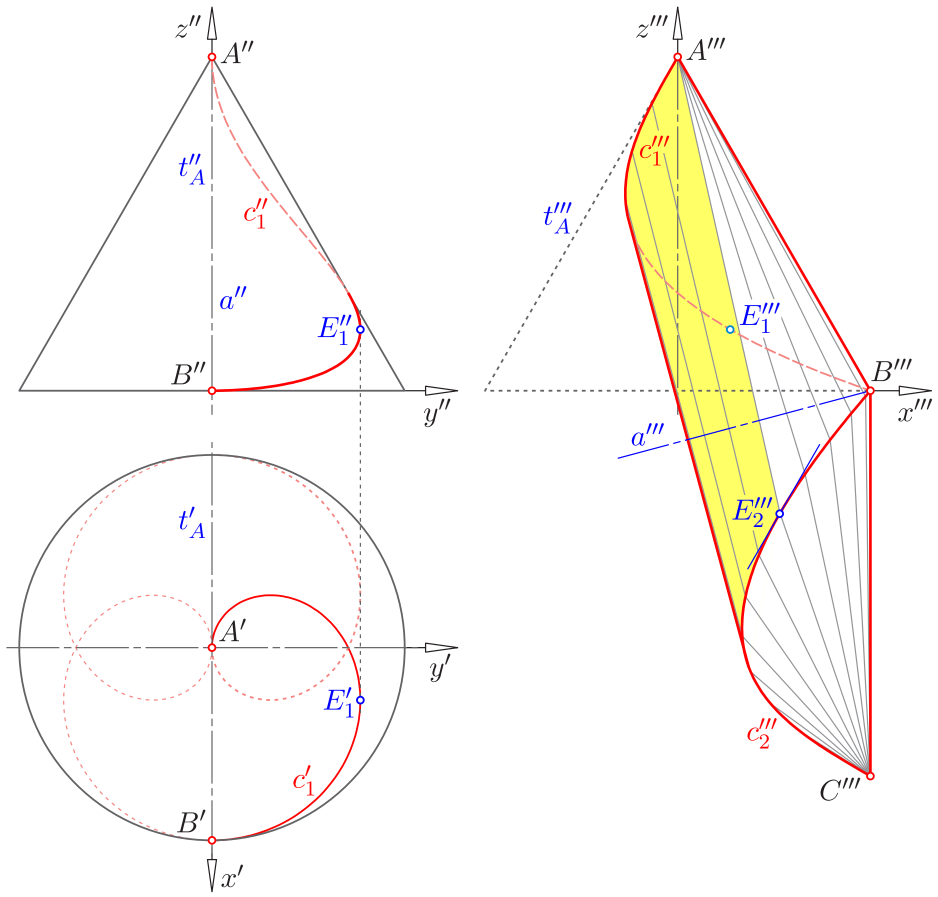


Figure 10: Approximation 1: $c_1$ is specified as a geodesic circle on a right cone

On the one hand, due to Lemma 4, 1., the half-rotation about the axis $a$ should map the tangent plane at $B = \mathbf{x}(\frac{\pi}{2})$ to the upper cone onto the rectifying plane of $c_1$, which is orthogonal to the principal normal $\mathbf{n}(\frac{\pi}{2})$. Therefore the slope of the axis $a$ in the $xz$-plane should be $(\sqrt{7} - \sqrt{3})/(5 + \sqrt{21})$, and hence the slope angle is approximately $5.447°$.

On the other hand, by virtue of Lemma 5, 1., the torse which connects the upper and the lower cone begins at the point $E_2 \in c_2$, whose tangent $t_{E_2}$ is parallel to the initial tangent $t_A$ (Figure 9). Hence, $t_{E_2}$ must be parallel to the $xz$-plane. In the same way, at the symmetric point $E_1 \in c_1$ the tangent $t_{E_1}$ is parallel to the final tangent $t_C$ of $c_2$ and to the $xz$-plane as well. Thus, for the point $E_1 = \mathbf{x}(\varphi_E)$ the second coordinate of the tangent vector $\mathbf{t}(\varphi_E)$ vanishes, hence $\sin\varphi_E = \sqrt{2/3}$ and $\cos\varphi_E = 1/\sqrt{3}$. Since the half-rotation about $a$ exchanges the direction of $t_{E_1}$ with that of $t_A$, the axis $a$ must have the slope $(\sqrt{3} - 1)/(\sqrt{3} + 1)$. The corresponding slope angle of $15°$ differs significantly from the value given before.

Anyway, Figure 10 shows in the side view the approximation of the required solid. The projections of the tangent indicatrices of $c_1$ and $c_2$ in the $xz$-plane (Figure 11) reveal that they have portions which are close together. However, by virtue of Lemma 5, 2., the tangent indicatrices of the subarcs $AE_1 \subset c_1$ and $E_2C \subset c_2$ should coincide.

We summarize:

*The assumption that the cone connecting $A$ with $c_1$ is a cone of revolution with the half apex angle $30°$ leads to an approximation which violates at least two of the conditions listed in Lemmas 4 and 5:*

- *At point $B$ the tangent plane to the lower cone with apex $C$ cannot be the rectifying*

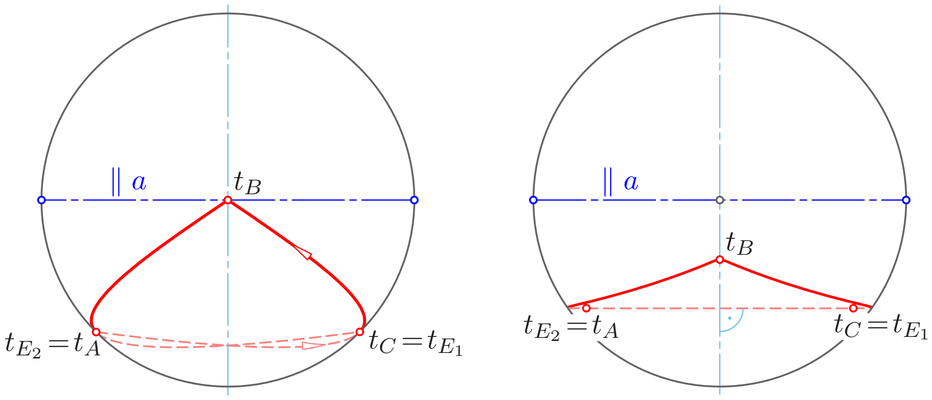


Figure 11: Tangent indicatrices of the curve $c$ in the approximations 1 (left, indicatrix of $c_1$ with arrows) and 2 (right) in a suitable projection into a plane through $a$

*plane of $c_1$, while the tangent $t_C$ to $c_2$ at the endpoint $C$ is parallel to the tangent $t_{E_1}$ to $c_1$ at $E_1$.*

- *The condition of coinciding tangent indicatrices, by virtue of Lemma 5, 2., is not precisely satisfied (note Figure 11, left).*

This first approximation has the property that $t_A$ and $t_C$ are located in the plane spanned by the axis $a$ and the two apices $A$ and $C$ which cannot be confirmed at the physical model. Furthermore, the angle $\sphericalangle ABC$ is about 150° while the physical model shows $\sim 131°$. This approximation has the volume $1.830\, r^3$ when $r$ is the radius of the semicircles in the given development (Figure 9).

## 2.2. Another approximation

By virtue of Lemma 5, 2., the tangent indicatrices of $c_1$ and $c_2$ should have identical subcurves. Our second approximation arises when we specify these portions such that they appear as a straight segment in the side view (note Figure 11, right). This means, the tangent indicatrix of these portions is a circular arc, the corresponding space curves are of *constant slope*. The rectifying torse is a *cylinder*.

Conversely, if the middle torse of $\Phi$ is supposed as a cylinder the arcs $AE_1$ and $E_2C$, being geodesics, are curves of constant slope w.r.t. generators $g$ of this cylinder. Then, in the development in Figure 9 all generators $g_0$ meeting the two straight segments of $c_0$ are parallel and of equal lengths. There is a *translation* along $g$ which maps the arc $AE_1 \subset c_1$ onto the arc $E_2C \subset c_2$. The half-rotation about the axis $a$ of symmetry maps $E_2C$ back to $E_1A$. Hence, there must be a *half-rotation about an axis* $a_1$ parallel to $a$ which exchanges $A$ with $E_1$ while the arc $AE_1$ is mapped onto itself.

This means, this slope curve has an axis $a_1$ of symmetry which meets $c_1$ at a point $F_1$. The axis $a_1$ must be orthogonal to the tangent plane of the cylinder at $F_1$ in order to guarantee that the complete arc $AE_1$ is a smooth slope curve. Since $E_1$ and $C$ are the images of $A$ under reflections in parallel axes $a_1$ and $a$, respectively, the points $A$, $C$, $E_1$, and $E_2$ lie in a plane orthogonal to $a$ (note the side view in Figure 12). On the other hand, the lines $AE_1$, $E_2C$ and the connection of $F_1$ with its translate $F_2$ are generators of the middle cylinder.

For a numerical approximation we use the same coordinate frame as in the first approximation. We specify an arbitrary slope angle $\psi$ which can be seen in the development as the slope angle of the generator $g_M$ (Figure 9). This defines the direction of the generators of

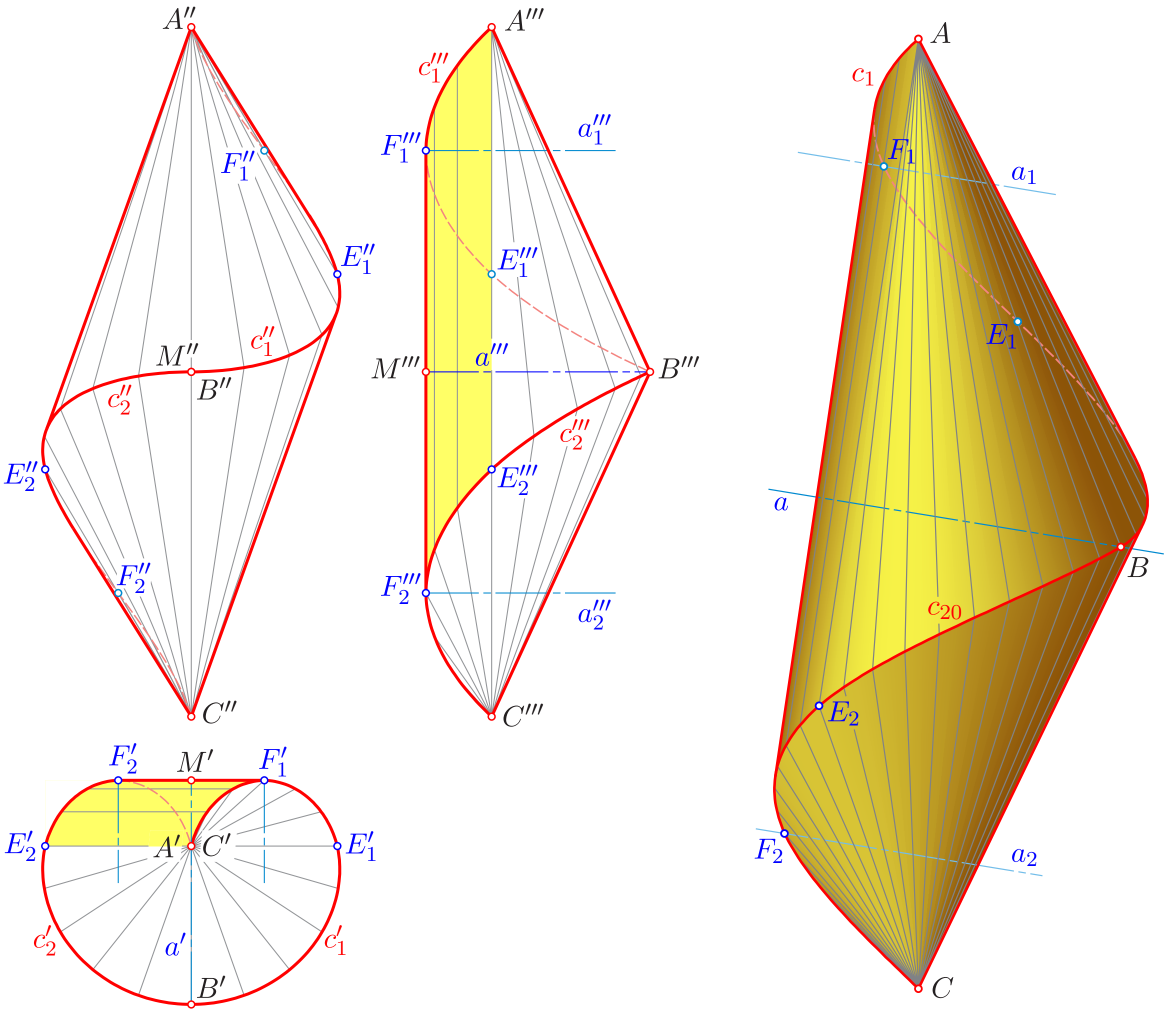


Figure 12: Example 2: Principal views with shaded cylindrical patch (left) and axonometry (right) of the second approximation

the cylinder, since the generator through $A$ lies in the diameter plane of the approximating right cone and makes with $t_A$ the angle $\psi$. Hence, $(90^\circ - \psi)$ is the constant slope angle of the initial portion of $c_1$. The angle $\psi$ defines the length of the translation $A \mapsto E_2$ as well as the length of the arc $AE_1$, which equals $\overline{A_0E'_{10}}$ in Figure 9.

The arc-length along $c_1$ between $A$ and $F_1$ is half of the length $AE_1$. We obtain the axis $a_1$ orthogonal to the tangent plane to the cylinder at $F_1$. On the generator of the cylinder through $F_1$ we find the central point $M$ with the axis $a$ passing through it. The axis $a$ is parallel to $a_1$ and contains the point $B$ in the distance $\overline{A_0B_0}$ to $A$.

During the numerical approximation of the arc $AF_1$ we have to note that for each point $X$ the distance to $A$ can be extracted from the development. Therefore, the length of the arc $AX$ along the curve $c_1$ of constant slope as well as the length of the chord $\overline{AX} = \overline{A_0X_0}$ is known. An orthogonal section $c_1^n$ of the rectifying cylinder (or the projection of $c_1$ in direction of the cylinder's generators) has the arc-length

$$\sigma = A^nX^n = 2r\varphi\sin\psi, \tag{7}$$

when $r$ denotes the radius of the semi-circles in the development and $2\varphi$ is the center angle — as in the first approximation. Then the length of the chord in the orthogonal section must

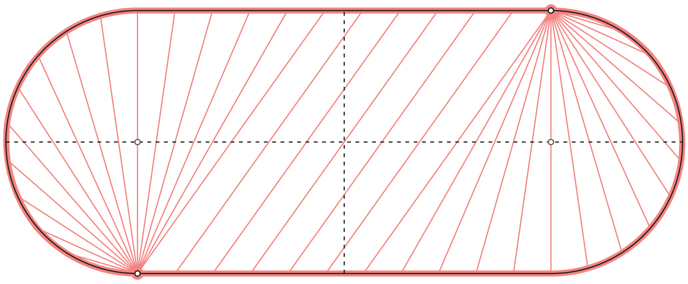

Figure 13: The development of the mathematical model (thick light red line) in comparison with the given development (thin black)

be

$$\overline{A^nX^n} = \sqrt{(2r\sin\varphi)^2 - (2r\varphi\ \cos\psi)^2}. \tag{8}$$

The remaining portion $E_1B$ of $c_1 \subset \Phi$ is the intersection of two cones. Its points $X$ have distances to $A$ and $C$ which are available in the development, i.e., $\overline{AX} = \overline{A_0X_0}$ for $X_0$ taken on the circular arc $E_{10}B_0$, and $\overline{CX} = \overline{C_0X_0'}$ for $X_0'$ on the segment $E_{10}'B_0'$ in Figure 9. Finally we vary the initial slope angle $\psi$ such that the computed curve $c_1$ ends exactly at the point $B$, which was already determined before.

This yields the following results: The optimal slope angle is approx. 54.53°, the 'width' $\overline{MB}$ of the solid, in terms of the radius $r$, is $1.18\,r$, the 'height' $\overline{AC} = 3.635\,r$, the angle $\sphericalangle ABC = 130.67°$, and the volume approx. $1.978\,r^3$. Figure 13 reveals that there is almost no difference between the development of this approximating mathematical model and the given development in Figure 9.

There is still a tiny contradiction inherent in this model: Since $a_1$ is the perpendicular bisector of $A$ and $E_1$, the distance $\overline{AE_1}$ is twice the distance between $A$ and the axis $a_1$. The condition $\overline{AE_1} = \overline{A_0E_{10}}$ implies that the right-angular triangle $A_0N_0F_{10}$ with $N_0$ as midpoint of $A_0E_{10}$ is congruent to the spatial counterpart $ANF_1$ with $N \in a_1$ (see Figure 14). On the other hand, the axis $a_1 = F_1N$ should be orthogonal to the tangent $t_F$ at $F$. At the model depicted in Figure 12 the angle between $a_1 = F_1N$ and the tangent $t_F$ is $\sim 88.84°$ Consequently, the tangent $t_{E_1}$ is not precisely parallel to $t_C$, but there is a discrepancy of $\sim 1.2°$.

We summarize:

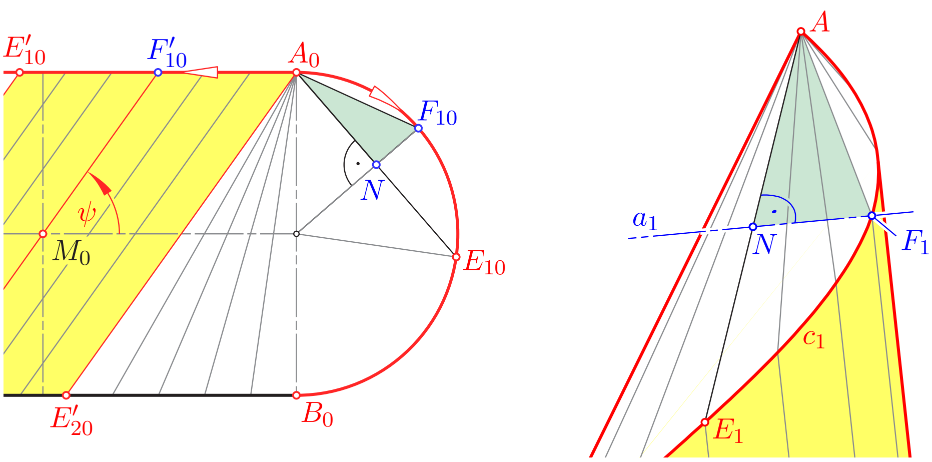


Figure 14: The triangle $ANF_1$ is congruent to its counterpart in the development

*The assumption that the central torsal patch of $\Phi$ is cylindric results in a good approximation (note Figure 12) of the physical model. However, it still differs from the theoretically correct version since the reflection of the initial arc $AF_1$ in $a_1$ gives an arc $E_1F_1$ which does not satisfy eq. (8) exactly.*

*Remark* 3. We can fold the sheet shown in Figure 9 in two ways, since we can choose the depicted side either in the interior of the solid or in the exterior. At the first choice the curve $c$ has negative torsion (like in the photo shown in Figure 8). Otherwise the helix-like curve is right-handed twisted, i.e., has a positive torsion (see Figure 12).

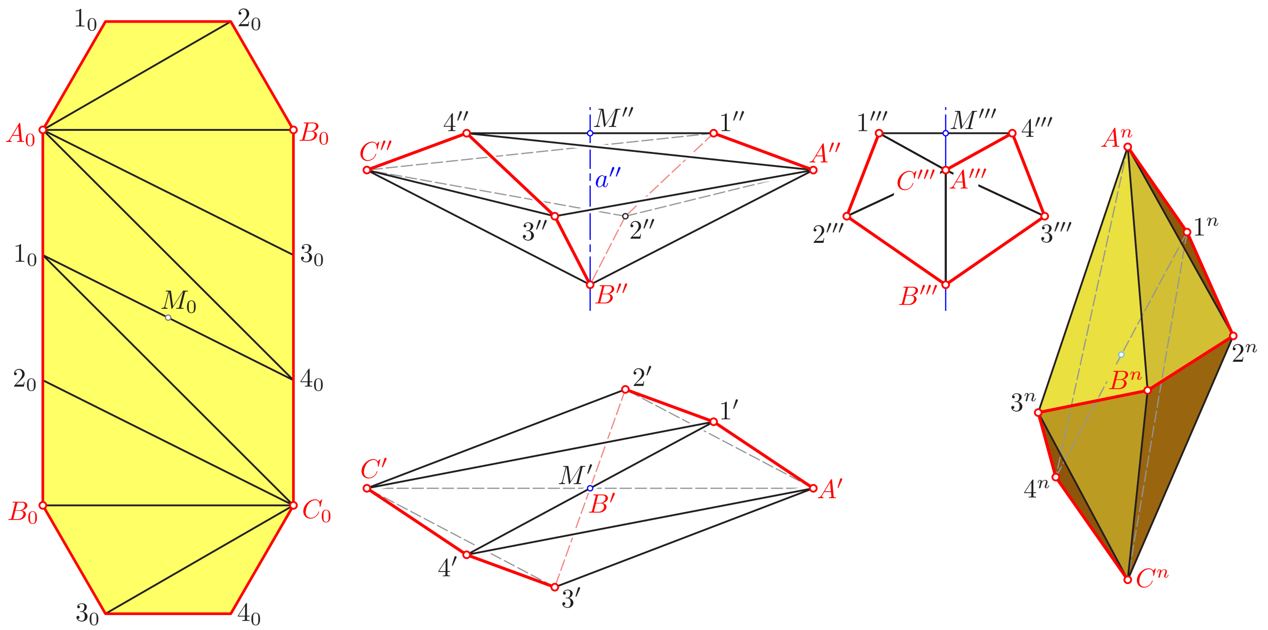


Figure 15: A discrete approximation of the solid: development (left) and spatial form in front, top and side view (middle) and in an axonometry (right)

*Remark* 4. When both semicircles in the development are replaced with halves of regular hexagons and the lengths of the straight segments $B_0C_0$ and $A_0D_0$ are chosen accordingly (Figure 15), we obtain a discrete model. It is a convex polyhedron with 7 vertices, 15 edges and 10 triangular faces. The existence of this polyhedron is also guaranteed by A. D. Alexandrov's famous *Uniqueness Theorem* (1941), since with the development a convex intrinsic metric is defined [1]. The two vertices $A$ and $C$ have degree 5, the remaining five degree 4. In terms of the side lengths $r$ of the polygon approximating the helix-like curve $c$, the 'width' $\overline{MB}$ of this polyhedron is about $1.5095\,r$, the 'height' $\overline{AC} = 3.557\,r$, the angle $\sphericalangle ABC = 125.56°$, and the volume $1.5485\,r^3$.

## Acknowledgement

The author thanks Georg Glaeser for the photos in Figure 8 and for pointing his attention to the interesting convex body, which was analysed in Section 2. Furthermore, the author appreciates the financial support received from the Austrian Academy of Sciences (ÖAW).

## References


[1] A.D. Alexandrov: *Convex Polyhedra*. Springer Monographs in Mathematics, Springer 2005 (first Russian edition 1950).

[2] M.P. do Carmo: *Differential Geometry of Curves and Surfaces*. Prentice-Hall Inc., Englewood Cliffs 1976.

[3] U. Bäsel, H. Dirnböck: *The Extended Oloid and Its Contacting Quadrics*. J. Geometry Graphics **19**/2, 161–177 (2015).

[4] H. Dirnböck: *Die Antizykloidenbewegung*. PhD Thesis, University of Klagenfurt/Austria 1986, Verlag Heyn, Klagenfurt 1987 (ISBN 3 85366 510 1).

[5] H. Dirnböck, H. Stachel: *The Development of the Oloid*. J. Geometry Graphics **1**, 105–118 (1997).

[6] L.P. Eisenhart: *An introduction to Differential Geometry*. Princeton University Press 1947.

[7] *Göttingen Collection of Mathematical Models and Instruments,* `http://modellsammlung.uni-goettingen.de`, accessed August 2016.

[8] M. Kilian, S. Flöry, Z. Chen, N.J. Mitra, A. Sheffer, H. Pottmann: *Curved Folding*. ACM Trans. Graphics **27**/3 (2008), Proc. SIGGRAPH 2008.

[9] E. Kreyszig: *Introduction to Differential Geometry and Riemannian Geometry*. University of Toronto Press 1967.

[10] J. Mitani: *Column-shaped Origami Design Based on Mirror Reflections*. J. Geometry Graphics **16**/2, 185–194 (2012).

[11] G. Scheffers: *Zusammenhang zwischen der Abwickelung eines Kreiscylinders und den Rotationsflächen konstanter Krümmung*. Arch. Math. Phys, III. Reihe, **6**, 249–250 (1903).

[12] K. Strubecker: *Differentialgeometrie III. Theorie der Flächenkrümmung*. Sammlung Göschen 1180/1180a, Walter de Gruyter & Co., Berlin 1959.

[13] W. Wunderlich: *Aufgabe 300*. El. Math. **22**, p. 89 (1957); author's solution: El. Math. **23**, 113–115 (1958).


Received August 6, 2016; final form November 23, 2016